Front. Chem. Sci. Eng. 2019, 13(4): 665–671
https://doi.org/10.1007/s11705-019-1815-2

COMMUNICATION

Plasmonic Au nanoparticles supported on both sides of TiO_2 hollow spheres for maximising photocatalytic activity under visible light

Jianwei Lu[1], Lan Lan[2], Xiaoteng Terence Liu (✉)[3], Na Wang (✉)[4], Xiaolei Fan (✉)[2]

1 School of Chemical Engineering and Technology, Collaborative Innovation Center of Chemical Science and Engineering, Tianjin University, Tianjin 300072, China
2 School of Chemical Engineering and Analytical Science, The University of Manchester, Manchester, M13 9PL, UK
3 Department of Mechanical & Construction Engineering, University of Northumbria, Newcastle upon Tyne, NE1 8ST, UK
4 Advanced Manufacturing Institute of Polymer Industry (AMIPI), Shenyang University of Chemical Technology, Shenyang 110142, China

Abstract A strategy of intensifying the visible light harvesting ability of anatase TiO_2 hollow spheres (HSs) was developed, in which both sides of TiO_2 HSs were utilised for stabilising Au nanoparticles (NPs) through the sacrificial templating method and convex surface-induced confinement. The composite structure of single Au NP yolk-TiO_2 shell-Au NPs, denoted as Au@Au(TiO_2, was rendered and confirmed by the transmission electron microscopy analysis. Au@Au(TiO_2 showed enhanced photocatalytic activity in the degradation of methylene blue and phenol in aqueous phase under visible light surpassing that of other reference materials such as Au(TiO_2 by 77% and Au@P25 by 52%, respectively, in phenol degradation.

Keywords TiO_2 hollow spheres, plasmonic Au nanoparticles, confinement, visible light, photocatalytic degradation

1 Introduction

Titanium dioxide is a semiconductor that has attracted increasing interests in photocatalytic and photovoltaic applications [1–4] because of the great oxidative potential of its positive holes ($E = +3.0$ V versus standard hydrogen electrode) [5], especially in the anatase form. However, due to the wide band-gap of 3.2 eV (for the anatase form) [6], TiO_2 has trivial response to the visible light (wavelength: 390–700 nm) [7,8] hindering the development of visible-light-driven photocatalysts based on TiO_2 for energy and environmental applications [6,9]. Various strategies [8,10–14] such as (i) metal (e.g., transition metals Cu, Co) [11] with and non-metal doping (e.g., *p*-block elements N, B, F) [12,15,16] and (ii) crystal structure and morphology engineering [13,14] are being developed to adjust the band structure and trap states of TiO_2 with an aim to enhance the response of the TiO_2-based photoelectrochemical materials in the visible region. Recently, the integration of plasmonic gold or silver nanoparticles (NPs) with TiO_2 [8,17–22] have been proposed to enhance the photocatalytic and photovoltaic activity in the visible region due to the strong surface plasmon resonance (SPR) excitation of such metal NPs, by which can enhance the concentration of charge carriers. One specific example presented by Zhang et al. [22] is the hybrid plasmonic Au nanoparticle (NP)-loaded hierarchical hollow porous TiO_2 spheres, which showed the enhanced the overall catalytic activity in 4-nitrophenol reduction [22]. In general, the energy-transfer mechanisms SPR were concluded as: (i) direct charge injection from metal to semiconductor, (ii) near-field electromagnetic and (iii) resonant photon-scattering mechanisms [21], depending largely on the geometric configuration of the composites. The synergic effect of plasmonic metal NPs and TiO_2 semiconductor can be manipulated by controlling the relative arrangement of the two building blocks. For instance, the electric field intensity enhancement was found dropped significantly by more than one order of magnitude when the distance between adjacent plasmonic Ag NPs were increased from 1 to 10 nm [21]. However, to stabilise nanosized metal particles on TiO_2 absorber against their high tendencies to aggregate presents a challenge to design stable hybrid nanostructures for practical settings. TiO_2 hollow spheres

Received November 27, 2018; accepted January 7, 2019

E-mails: terence.liu@northumbria.ac.uk (Liu X T),
iamwangna@syuct.edu.cn (Wang N),
xiaolei.fan@manchester.ac.uk (Fang X)

(HSs) [20,23,24] have attracted increasing interests due to their tunable structural properties (e.g., size, shell thickness and crystallinity) and hence their photoelectrochemical properties [23,24]. The unique void of TiO_2 HSs was also employed to encapsulate and stabilise plasmonic metal NPs [17,20,25−27] yielding yolk (metal NP)-shell (TiO_2) arrangements, e.g., Au(TiO_2 HSs ('(' represents the encapsulation of Au NP in HSs), with improved thermal stability of the metal cores. Though few excellent samples of the yolk-shell Au(TiO_2 HSs nanoreactors have shown good performance in photocatalytic oxidation of CO [20] and water splitting [26], their applications in liquid phase environmental remediation with bigger organic molecules are still limited due to (i) the restricted accessibility of the metal core and (ii) the inadequate availability of metal species (usually the single core configuration was designed to avoid aggregation).

Molecular dynamics simulations have shown that the surface layer of a metal NP possessed liquidlike properties [28] favouring the aggregation of adjacent metal NPs. In fact, the outer surface of TiO_2 HSs is convex in all directions perfect to provide spatial confinement for separating metal drops. To date, the confinement effect of metal NPs created by the curvature of the TiO_2 HSs has been mostly neglected, and only a few examples showed the effectiveness of using the outer surface of TiO_2 HSs to stabilise plasmonic metal NPs [8]. Herein, we demonstrate the design and synthesis of plasmonic Au-TiO_2 HSs nanostructure with Au NPs deposited on both sides of the anatase TiO_2 HS, i.e., a single encapsulated Au core and multiple Au NPs confined by the convex curved outer surface of the TiO_2 HS, denoted as Au@Au(TiO_2 (@ represents the deposition of Au NP on HSs), to improve the photocatalytic efficiency of the system.

2 Materials and methods

2.1 Synthesis of core-shell Au(SiO_2

All glassware was thoroughly cleaned with aqua regia (three parts HCl, one part HNO_3) for 12 h and rinsed with deionised water (DI). 5 mL sodium citrate (1%, Tianjin Chemical Reagent No 1 Plant) was dispersed into 50 mL $HAuCl_4 \cdot 3H_2O$ (J&K Scientific) aqueous solution (4×10^{-4} mol/L) under sonication and then heated to 95°C. After 5 min, 37.5 mL of 400 mmol/L myristyltrimethylammonium bromide (TTAB, Sigma-Aldrich, ⩾99%) was added to the solution and the mixture was maintained at 95°C for 15 min under vigorous stirring. The obtained TTAP-capped Au aqueous solution (20 mL), tetraethyl orthosilicate (28%, Tianjin Chemical Reagent No 1 Plant, 0.96 mL), dehydrated ethanol (99.8%, Tianjin Guangfu Fine Chemical Institute, 23 mL) and ammonia solution (26%, Tianjin Guangfu Fine Chemical Institute, 0.62 mL) were then mixed and stirred for 4 h at room temperature. The precipitated silica nanoparticles were extracted by centrifugal separation and washed with ethanol then re-dispersed in 5 mL of ethanol.

2.2 Synthesis of yolk-shell Au(TiO_2

Au(SiO_2 was dispersed in a mixture of hydroxypropyl cellulose (HPC, Tokyo Chemical Industry Co., Ltd., 0.1 g), ethanol (20 mL) and DI (0.1 mL) and stirred for 40 min. Titanium tert-butoxide (98%, Tianjin Chemical Reagent No 1 Plant, 1 mL) in ethanol (5 mL) solution was added in the mixture at a rate of 0.5 mL/min. The mixture was stirred at 900 r/min and 85°C under refluxing condition for 100 min. The final product was separated by centrifugation, washed with ethanol, and kept in 5 mL of ethanol to form Au (SiO_2(TiO_2 nanocomposites. The Au(SiO_2(TiO_2 was calcined in air at 500°C (2°C/min) for 2 h to remove all organic compounds and crystallise the amorphous TiO_2. The calcined samples were dispersed in 20 mL water under sonication and heated to 50°C. 1.5 mL aqueous NaOH solution (2.5 mol/L, Tianjin Guangfu Fine Chemical Institute) was added in the aqueous Au(SiO_2(TiO_2 solution and the solution was heated to 70°C. Finally, aqueous NaOH solution (2.5 mol/L, 1 mL) was added and the resulting solution was stirred for 6 h to remove the SiO_2 core and obtain yolk-shell Au(TiO_2.

2.3 Synthesis of Au@Au(TiO_2

Yolk-shell Au(TiO_2 (0.1 g) and sodium citrate (1%, Tianjin Chemical Reagent No 1 Plant, 5 mL) were dispersed into 50 mL $HAuCl_4 \cdot 3H_2O$ aqueous solution (4×10^{-4} mol/L) under sonication. The mixture was heated to 95°C and maintained at 95°C for 20 min under vigorous stirring. The product was separated by centrifugal separation, washed with DI and dried at 100°C for 10 h. The same procedure was used for depositing Au NPs on other supports.

2.4 Characterisation of materials

N_2 adsorption-desorption at −196°C was performed using a Micromeritics Tristar 3000 analyser to determine the specific surface area (the Brunauer–Emmett–Teller method) and the pore size distribution (the Barrett-Joyner-Halenda method). X-ray diffraction (XRD) patterns of materials were recorded on a Bruker D8 Focus diffractometer (nickel-filtered Cu$K\alpha$1 radiation, λ = 1.5406 Å, 40 kV, 40 mA) at a scanning rate of 0.02° per step and 0.15 s per step in a 2θ range of 10°−85° (and 5°−65°). Transmission electron microscopy (TEM) imaging was completed using an FEI Tecnai G2 F20 operating at 100 kV. Samples were dispersed in ethanol and pipetted onto the copper grid-supported transparent carbon foil and dried prior to imaging. Scanning electron microscopy imaging of materials was undertaken using a JEM-2100F. Diffuse reflectance spectra (DRS) of materials were

obtained using a SHIMADZU UV-2550 spectrophotometer equipped with a 60 nm diameter integrating sphere using $BaSO_4$ as the reflectance sample.

2.5 Evaluation of photocatalytic activity

The photocatalytic activity of materials was evaluated by photodegradation of methylene blue (MB, 98%, Tianjin Damao Chemical Co., Ltd.) and phenol (Tianjin Damao Chemical Co., Ltd.). 50 mg photocatalyst was firstly added into a 100 mL quartz photoreactor containing the solution with the substrate (12 mmol/L) and ultrasonicated for 2 min. The mixture was magnetically stirred for 30 min in the dark to ensure good dispersion of the photocatalyst in the solution the adsorption-desorption equilibrium between substrate molecules and the photocatalyst. The same 50 mg photocatalyst was also used for phenol solution (100 μmol/L). A visible light source ($420 \leqslant \lambda \leqslant 780$ nm) was introduced by a 300 W xenon lamp (Beijing Perfectlight Technology Co. Ltd., LS-SXE300-CUV, equipped with an AM 1.5-filter power intensity = 100 mW/cm^2) 10 cm above the liquid surface. The ambient temperature of the reaction was maintained by water cooling during the reaction. Every 30 min, a 2 mL sample was taken and analysed for the concentration of the substrate. For MB and phenol, the absorbance intensity at their maximum absorbance wavelength of λ_{max} = 664, 270 nm was monitored using a SHIMADZU UV-2550 spectrophotometer.

3 Results and discussion

The synthesis and morphological evolution of the yolk-shell Au(TiO_2 nanostructure and the corresponding TEM images were illustrated in Figs. 1 and 2. A three-step method was used (Fig. 1) to synthesise the yolk-shell Au(TiO_2 nanostructure, i.e., (i) Synthesising Au(SiO_2 nanoparticles using the Stöber method (Fig. 2(a)) [29]; (ii) Coating Au(SiO_2 with anatase TiO_2 via hydrolysis-condensation and calcination (Fig. 2(b)) [17,23]; and (iii) Removing SiO_2 core to render the yolk-shell Au(TiO_2 with NaOH-based chemical etching (Fig. 2(c)). The method enabled the solitary inclusion of one myristyltrimethylammonium bromide-capped Au NP of 7±2 nm. The average shell thickness and diameter of the anatase TiO_2 shell are about 25±2 and 140±10 nm, respectively. The developed TiO_2 shell was highly porous with a specific surface area of 187 m^2/g (Figs. S1, S2 and Table S1, cf. Electronic Supplementary Material (ESM)).

To further utilise the outer surface of the porous TiO_2 shell, Au NPs (ca. 1 wt-%) were deposited on the yolk-shell Au(TiO_2 yielding the Au NP core-TiO_2 shell-Au NPs hybrid structure as shown in Fig. 2(d). Au NPs with similar diameters were found well-dispersed on the outer surface of anatase TiO_2 shell in the as-prepared Au(TiO_2 (Fig. 2(d)). The convex outer surface of TiO_2 HSs was believed to avoid the aggregation of Au NPs. High-resolution transmission electron microscopy (HR-TEM) analysis also showed the well-resolved crystalline Au NPs with a fine crystal lattice spacing of 0.2355 nm (inset of Fig. 2(d)), corresponding to (111) plane of the face-centred cubic gold. For the purpose of comparison, TEM images of pure SiO_2 core, core-shell SiO_2(TiO_2, TiO_2 HSs and Au@TiO_2 HSs were prepared and shown in Figs. 2(e–h). It was found that the hollow spherical structure of porous TiO_2 remained largely intact during the synthesis (Fig. S1). XRD patterns of TiO_2 HSs, Au@TiO_2, Au(TiO_2 and Au@Au(TiO_2 (Fig. S3, cf. ESM) showed characteristic diffraction peaks of the anatase TiO_2 phase (JCPDS file no. 21-1272) and the Au metal phase (JCPDS file no. 01-1174). As compared to Au(TiO_2, the intensity of Au peaks in Au@Au(TiO_2 are much stronger, which can be attributed to the extra Au NPs loaded on TiO_2 shell. UV-Vis DRS analyses (Fig. S4, cf. ESM) showed that there was no absorption observed in the visible region for TiO_2 HSs. With the decoration of plasmonic Au NPs, the surface plasmon resonance (SPR) peaks at around 550 nm emerged [30,31]. In comparison with pure Au nanocrystal (ca. 520 nm), the redshift in SPR peaks of Au-based TiO_2

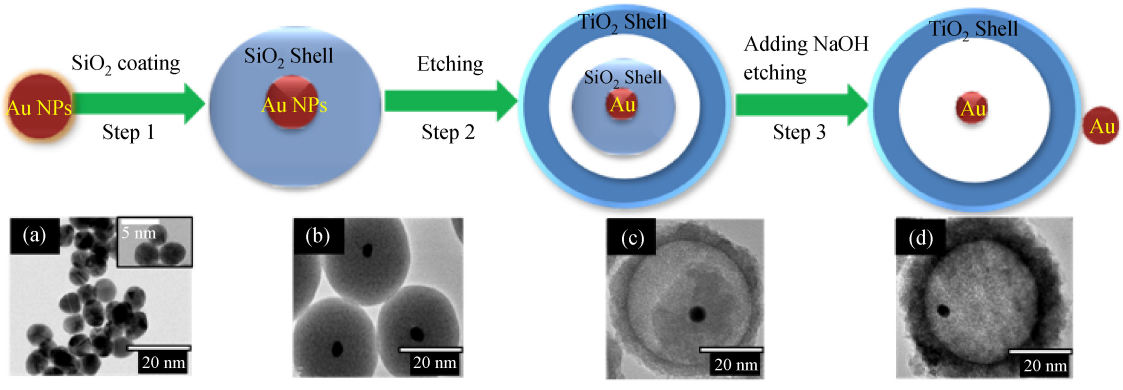

Fig. 1 Scheme of synthesis and formation of the single Au core-anatase TiO_2 shell nanostructure. (a–d) TEM images showing the morphological evolution of the yolk-shell Au(TiO_2

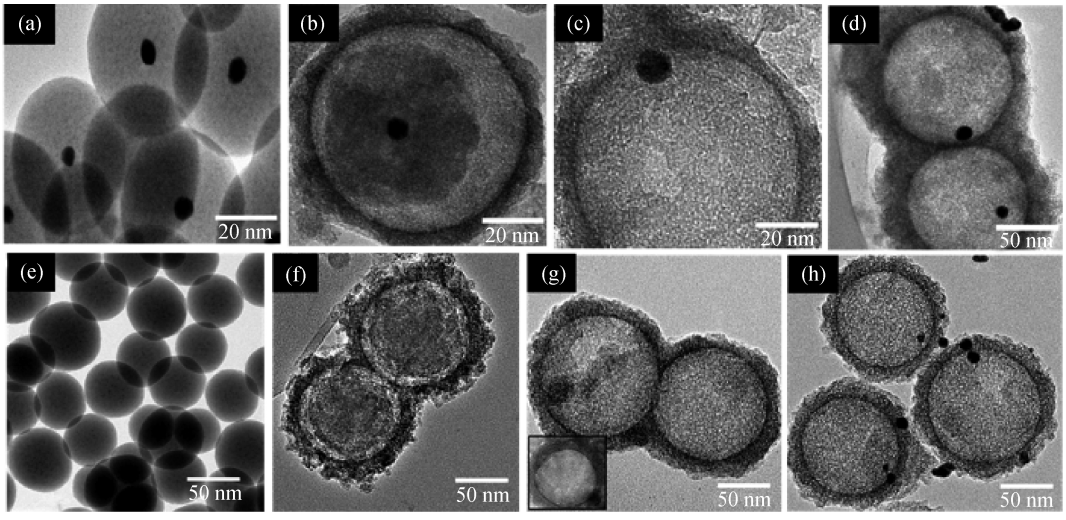

Fig. 2 TEM images of the as-prepared materials: (a) Au(SiO_2, (b) core-core-shell Au(SiO_2(TiO_2, (c) yolk-shell Au(TiO_2, (d) Au@Au (TiO_2, (e) SiO_2 core, (f) SiO_2(TiO_2 core-shell, (g) TiO_2 HSs, (h) Au@TiO_2 HSs

materials can be ascribed to the effect of the high-refractive-index anatase TiO_2 shell [32,33]. In addition, the variation in SPR intensities found in Au-based TiO_2 composites (Au@Au(TiO_2, Au(TiO_2 and Au@TiO_2) suggests that the optical properties of TiO_2 HSs can be tuned by controlling the deposition location of Au NPs. Yolk-shell Au@Au(TiO_2 showed the strongest SPR intensity among these samples, which is related to a substantial increase in its scattering coefficient promoted by the Au NPs located on both sides of TiO_2 shell. The photocatalytic activity of materials was evaluated under visible light irradiation ($420 \leqslant \lambda \leqslant 780$ nm) using MB and phenol as probe molecules shown in Figs. 3 and 4.

Comparative photocatalytic studies were carried out using materials developed alongside naked Au NPs and Au NPs supported on P25 catalyst (Au@P25) and results were shown in Figs. 3(a) and 4(a). The chemical catalysis effect of Au NPs was trivial because naked Au NPs were found inactive in both cases. Commercial P25 and TiO_2 HSs showed the poor catalytic activity with both MB and phenol (i.e., $< 7\%$ conversions after 180 min illumination) suggesting that the plasmon-enhanced light absorption and plasmonic sensitisation of Au NPs indeed improved the photocatalytic activity of TiO_2 materials. Au@TiO_2 HSs showed better activities than Au@P25 in both photocatalytic model reactions. This is attributed to the high specific surface area of TiO_2 HSs (187 m^2/g) providing abundant active sites for converting the probing molecules, while only 36 m^2/g for commercial P25 (Table S1). In addition, the light harvesting and scattering ability were

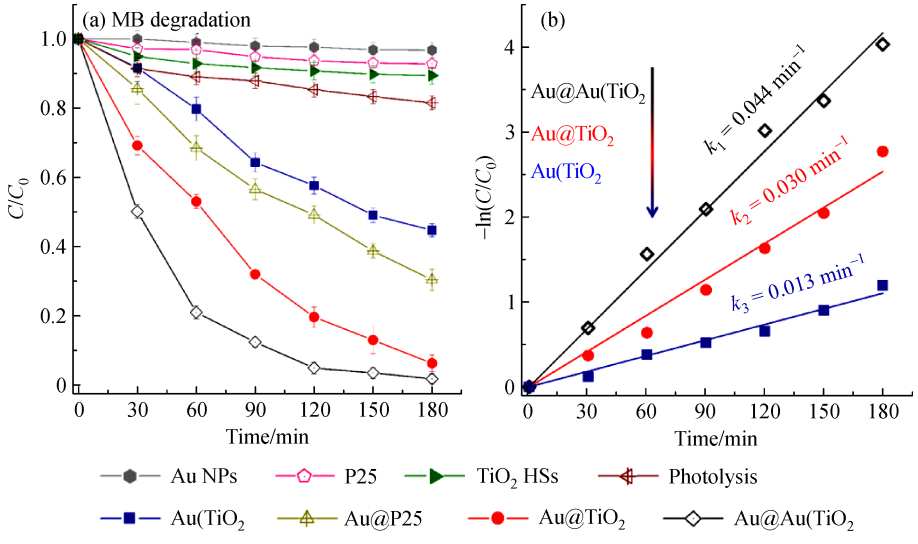

Fig. 3 (a) The rate of MB degradation under visible light promoted by various TiO_2 photocatalysts; (b) The corresponding pseudo-first-order kinetic rate plot

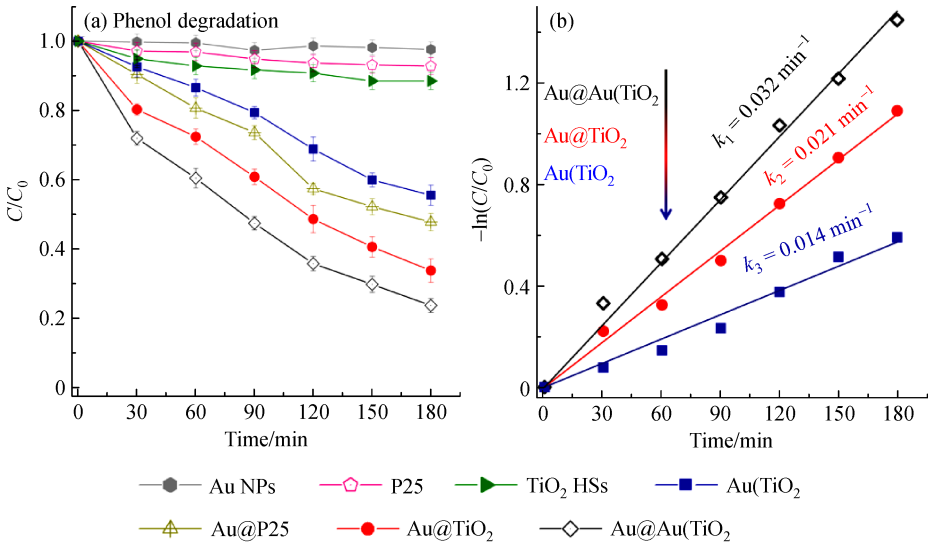

Fig. 4 (a) The rate of phenol degradation under visible light promoted by various TiO_2 photocatalysts; (b) The corresponding pseudo-first-order kinetic rate plot

also improved by the HSs structure as explained in the previous work [17]. For the Au-based TiO_2 hybrid nanomaterial, the decolorisation of MB and degradation of phenol were improved for the same period of the time, following the order of activity as: Au@Au(TiO_2 > Au@TiO_2 HSs > yolk-shell Au(TiO_2.

The degradation rate of both probing molecules followed first-order kinetics concerning their concentrations. The rate can, therefore, be interpreted using the pseudo-first-order reaction model (Figs. 3(b) and 4(b)). The previous study by the action spectrum has shown that the degradation of MB was induced mainly by the SPR excitation of Au NPs in Au-TiO_2 materials rather than the sensitisation of the dye molecules [30]. By comparing the rate constants in the decolourisation of MB, Au@TiO_2 HSs showed a better activity (0.030 min^{-1}) than that of yolk-shell Au(TiO_2 (0.013 min^{-1}). In the yolk-shell Au(TiO_2, e–h pairs are produced inside the TiO_2 shell, whereas the catalytic reactions take place mostly at the outer surface of TiO_2 HSs. Therefore, the transportation of e–h pairs through the TiO_2 shell increases the probability of e–h recombination leading to the relatively low activity in photocatalysis in comparison with that of Au@TiO_2 HSs. To decorate the inner and outer surface of TiO_2 HSs simultaneously, the photocatalytic activity of Au@Au(TiO_2 increased significantly with a constant of 0.044 min^{-1} for MB decolourisation, more than three times higher than that of yolk-shell Au(TiO_2. Based on the results above, the utilisation of both sides of TiO_2 shell was proven to be efficient to boost the photocatalytic activity of Au NP-TiO_2 HS nanostructures. This can be attributed mainly to the improved light-harvesting capacity of TiO_2 HSs caused by the multiple intensified local electromagnetic fields across the TiO_2 shell. Accordingly, the interfacial hot electron transfer from Au NPs to TiO_2 shell upon the excitation of the LSPR (plasmonic sensitisation) was also intensified effectively as the synergistic effect. Additionally, due to the confinement of Au NPs both within the TiO_2 HSs and on their convex external surfaces, the developed Au@Au(TiO_2 photocatalyst also demonstrated good stability in the model reaction. The photocatalyst remained sufficiently active even after three successive recycles in the decolourisation of MB in the aqueous phase (Fig. S5, cf. ESM)

4 Conclusions

In conclusion, a hybrid structure of Au nanoparticles (NPs) and anatase TiO_2 HSs was synthesised, in which Au NPs were confined on both sides of the TiO_2 HSs enabled by the silica templating-NaOH etching and convex surface-induced confinement. The sandwich yolk-shell structures of Au NPs and TiO_2 HSs, termed Au@Au(TiO_2, were determined by TEM characterisation, in which multiple Au NPs decorated on a single Au yolk-TiO_2 shell nanostructure were found. According to the UV-Vis DRS analysis, Au@Au(TiO_2 showed the strongest SPR intensity at about 550 nm compared to Au(TiO_2 and Au@TiO_2. Comparative studies of Au@Au(TiO_2, Au(TiO_2, Au@TiO_2 and Au@P25 in the photocatalytic degradation of two model molecules (i.e., MB and phenol) under visible light irradiation were carried out. Au@Au(TiO_2 exhibited the enhanced activity for both reactions with the degradation rate of MB and phenol as 99% and 78%, respectively, after 180 min due to the multiple intensified local electromagnetic fields across the TiO_2 shell. The strategy of sequential decorating both sides of TiO_2 shells

is generic and applicable to another semiconductor hollow spherical materials (e.g., $BiVO_4$ and SnO_2), which is beneficial to develop highly efficient photocatalysts for photoelectrochemical applications such as solar cells and water splitting.

Acknowledgements We thank for the financial support from The University of Manchester through Higher Education Innovation Funded 'Knowledge and Innovation Hub for Environmental Sustainability'. LL thanks the China Scholarship Council (CSC, file no. 201706950035)-University of Manchester joint studentship for supporting her Ph.D. research.

Electronic Supplementary Material Supplementary material is available in the online version of this article at https://doi.org/10.1007/s11705-019-1815-2 and is accessible for authorized users.

References

1. Schrauben J N, Hayoun R, Valdez C N, Braten M, Fridley L, Mayer J M. Titanium and zinc oxide nanoparticles are proton-coupled electron transfer agents. Science, 2012, 336(6086): 1298–1301
2. Gratzel M. Photoelectrochemical cells. Nature, 2001, 414(6861): 338–344
3. Caravaca A, Daly H, Smith M, Mills A, Chansai S, Hardacre C. Continuous flow gas phase photoreforming of methanol at elevated reaction temperatures sensitised by Pt/TiO_2. Reaction Chemistry & Engineering, 2016, 1(6): 649–657
4. Caravaca A, Jones W, Hardacre C, Bowker M H. Hydrogen production by the photocatalytic reforming of cellulose and raw biomass using Ni, Pd, Pt and Au on titania. Proceedings of the Royal Society A: Mathematical, Physical and Engineering Science, 2016, 472
5. Palmisano L, Sclafani A. Thermodynamics and kinetics for heterogeneous photocatalytic processes. In: Schiavello M, ed. Heterogeneous Photocatalysis. New York: John Wiley & Sons, 1997, 109–132
6. Cong Y, Zhang J, Chen F, Anpo M. Synthesis and characterization of nitrogen-doped TiO_2 nanophotocatalyst with high visible light activity. Journal of Physical Chemistry C, 2007, 111(19): 6976–6982
7. Meng Q, Wang T, Liu E, Ma X, Ge Q, Gong J. Understanding electronic and optical properties of anatase TiO_2 photocatalysts co-doped with nitrogen and transition metals. Physical Chemistry Chemical Physics, 2013, 15(24): 9549–9561
8. Lu J, Su F, Huang Z, Zhang C, Liu Y, Ma X, Gong J. *N*-Doped Ag/TiO_2 hollow spheres for highly efficient photocatalysis under visible-light irradiation. RSC Advances, 2013, 3(3): 720–724
9. Wang H, Zhang L, Chen Z, Hu J, Li S, Wang Z, Liu J, Wang X. Semiconductor heterojunction photocatalysts: Design, construction, and photocatalytic performances. Chemical Society Reviews, 2014, 43(15): 5234–5244
10. Pan H, Zhang Y W, Shenoy V B, Gao H. Effects of *H*-, *N*-, and (*H*, *N*)-doping on the photocatalytic activity of TiO_2. Journal of Physical Chemistry C, 2011, 115(24): 12224–12231
11. Pelaez M, Nolan N, Pillai S, Seery M, Falaras P, Patrick A G, Jeremy S M, Hamiltone W J, Byrne J A, O'Shea K, et al. A review on the visible light active titanium dioxide photocatalysts for environmental applications. Applied Catalysis B: Environmental, 2012, 125: 331–349
12. Dozzi M V, Selli E. Doping TiO_2 with *p*-block elements: Effects on photocatalytic activity. Journal of Photochemistry and Photobiology C, Photochemistry Reviews, 2012, 14: 13–28
13. Kamat P V. TiO_2 nanostructures: Recent physical chemistry advances. Journal of Physical Chemistry C, 2012, 116(22): 11849–11851
14. Li L, Yan J, Wang T, Zhao Z J, Zhang J, Gong J, Guan N. 10 nm rutile titanium dioxide nanoparticles for efficient visible-light-driven photocatalytic hydrogen production. Nature Communications, 2015, 6(1): 5881
15. Ansari S A, Khan M M, Ansari M O, Cho M H. Nitrogen-doped titanium dioxide (*N*-doped TiO_2) for visible light photocatalysis. New Journal of Chemistry, 2016, 40(4): 3000–3009
16. Li L, Meng F, Hu X, Qiao L, Sun C Q, Tian H, Zheng W. TiO_2 band restructuring by B and P dopants. PLoS One, 2016, 11(4): e0152726
17. Lu J, Zhang P, Li A, Su F, Wang T, Liu Y, Gong J. Mesoporous anatase TiO_2 nanocups with plasmonic metal decoration for highly active visible-light photocatalysis. Chemical Communications (Cambridge), 2013, 49(52): 5817–5819
18. Tian Y, Tatsuma T. Mechanisms and applications of plasmon-induced charge separation at TiO_2 films loaded with gold nanoparticles. Journal of the American Chemical Society, 2005, 127(20): 7632–7637
19. Awazu K, Fujimaki M, Rockstuhl C, Tominaga J, Murakami H, Ohki Y, Yoshida N, Watanabe T. A plasmonic photocatalyst consisting of silver nanoparticles embedded in titanium dioxide. Journal of the American Chemical Society, 2008, 130(5): 1676–1680
20. Lee I, Joo J B, Yin Y D, Zaera F. A yolk@shell nanoarchitecture for Au/TiO_2 catalysts. Angewandte Chemie International Edition, 2011, 50(43): 10208–10211
21. Linic S, Christopher P, Ingram D B. Plasmonic-metal nanostructures for efficient conversion of solar to chemical energy. Nature Materials, 2011, 10(12): 911–921
22. Zhang Q, Jin X, Xu Z, Zhang J, Rendón U F, Razzari L, Chaker M, Ma D. Plasmonic Au-loaded hierarchical hollow Porous TiO_2 spheres: Synergistic catalysts for nitroaromatic reduction. Journal of Physical Chemistry Letters, 2018, 9(18): 5317–5326
23. Joo J B, Dahl M, Li N, Zaera F, Yin Y. Tailored synthesis of mesoporous TiO_2 hollow nanostructures for catalytic applications. Energy & Environmental Science, 2013, 6(7): 2082–2092
24. Joo J B, Zhang Q, Dahl M, Lee I, Goebl J, Zaera F, Yin Y. Control

of the nanoscale crystallinity in mesoporous TiO_2 shells for enhanced photocatalytic activity. Energy & Environmental Science, 2012, 5(4): 6321–6327

25. Dillon R J, Joo J B, Zaera F, Yin Y, Bardeen C J. Correlating the excited state relaxation dynamics as measured by photoluminescence and transient absorption with the photocatalytic activity of Au@TiO_2 core-shell nanostructures. Physical Chemistry Chemical Physics, 2013, 15(5): 1488–1496
26. Lee Y J, Joo J B, Yin Y, Zaera F. Evaluation of the effective photoexcitation distances in the photocatalytic production of H_2 from water using Au@void@TiO_2 yolk-shell nanostructures. ACS Energy Letters, 2016, 1(1): 52–56
27. Lee I, Joo J B, Yin Y, Zaera F. Au@Void@TiO_2 yolk-shell nanostructures as catalysts for the promotion of oxidation reactions at cryogenic temperatures. Surface Science, 2016, 648: 150–155
28. José-Yacamán M, Gutierrez-Wing C, Miki M, Yang D Q, Piyakis K N, Sacher E. Surface diffusion and coalescence of mobile metal nanoparticles. Journal of Physical Chemistry B, 2005, 109(19): 9703–9711
29. Liz-Marzan L M, Giersig M, Mulvaney P. Synthesis of nanosized gold-silica core-shell particles. Langmuir, 1996, 12(18): 4329–4335
30. Bian Z, Tachikawa T, Zhang P, Fujitsuka M, Majima T. Au/TiO_2 Superstructure-based plasmonic photocatalysts exhibiting efficient charge separation and unprecedented activity. Journal of the American Chemical Society, 2014, 136(1): 458–465
31. Prikulis J, Hanarp P, Olofsson L, Sutherland D, Käll M. Optical spectroscopy of nanometric holes in thin gold films. Nano Letters, 2004, 4(6): 1003–1007
32. Seh Z W, Liu S H, Low M, Zhang S Y, Liu Z L, Mlayah A, Han M Y. Janus Au-TiO_2 photocatalysts with strong localization of plasmonic near-fields for efficient visible-light hydrogen generation. Advanced Materials, 2012, 24(17): 2310–2314
33. Wu X F, Song H Y, Yoon J M, Yu Y T, Chen Y F. Synthesis of core-shell Au@TiO_2 nanoparticles with truncated wedge-shaped morphology and their photocatalytic properties. Langmuir, 2009, 25 (11): 6438–6447